2012

# Continually adjustable oriented 1D TiO2 nanostructure arrays with controlled growth of morphology and their application in dye-sensitized solar cells

Ziqi Sun
*University of Wollongong*, ziqi@uow.edu.au

Jung Ho Kim
*University of Wollongong*, jhk@uow.edu.au

Ting Liao
*The University Of Queensland,University Of Queensland*

Yue Zhao
*University of Wollongong*, yue_zhao@uow.edu.au

Fargol Bijarbooneh
*University Of Wollongong*

*See next page for additional authors*

View Online / Journal Homepage / Table of Contents for this issue
Dynamic Article Links

CrystEngComm

Cite this: *CrystEngComm*, 2012, **14**, 5472–5478

www.rsc.org/crystengcomm

**PAPER**

# Continually adjustable oriented 1D $TiO_2$ nanostructure arrays with controlled growth of morphology and their application in dye-sensitized solar cells†

**Ziqi Sun,[a] Jung Ho Kim,*[a] Ting Liao,[b] Yue Zhao,[a] Fargol Bijarbooneh,[a] Victor Malgras[a] and Shi Xue Dou[a]**

***Received 5th January 2012, Accepted 13th March 2012***
**DOI: 10.1039/c2ce00014h**



Oriented, single-crystalline, one-dimensional (1D) $TiO_2$ nanostructures would be most desirable for providing fascinating properties and features, such as high electron mobility or quantum confinement effects, high specific surface area, and even high mechanical strength, but achieving these structures has been limited by the availability of synthetic techniques. In this study, a concept for precisely controlling the morphology of 1D $TiO_2$ nanostructures by tuning the hydrolysis rate of titanium precursors is proposed. Based on this innovation, oriented 1D rutile $TiO_2$ nanostructure arrays with continually adjustable morphologies, from nanorods (NRODs) to nanoribbons (NRIBs), and then nanowires (NWs), as well as the transient state morphologies, were successfully synthesized. The proposed method is a significant finding in terms of controlling the morphology of the 1D $TiO_2$ nano-architectures, which leads to significant changes in their band structures. It is worth noting that the synthesized rutile NRIBs and NWs have a comparable bandgap and conduction band edge height to those of the anatase phase, which in turn enhances their photochemical activity. In photovoltaic performance tests, the photoanode constructed from the oriented NRIB arrays possesses not only a high surface area for sufficient dye loading and better light scattering in the visible light range than for the other morphologies, but also a wider bandgap and higher conduction band edge, with more than 200% improvement in power conversion efficiency in dye-sensitized solar cells (DSCs) compared with NROD morphology.

## Introduction

Titanium dioxide, $TiO_2$, has been recognized as one of the most promising semiconductor materials for photovoltaic, photocatalytic, and sensing applications, owing to its wide band gap, environmental friendliness, and cost-effectiveness.[1] With rising interest in engineering the morphology of semiconducting materials during the last decade, the performance of $TiO_2$-based devices is known to be affected by not only the electronic structure, but also the shape and size of the $TiO_2$.[1] For example, the performance of DSCs, measured in terms of power conversion efficiency, depends closely on the light harvesting capacities of the dye adsorbed on the $TiO_2$ photoanode, the transport of the photoinjected electrons through the semiconductor electrode, and the dynamics of interfacial losses resulting from the possible recombination of electrons with either the oxidized dye or the oxidized electrolyte species produced upon regeneration of the oxidized sensitizer.[2] Therefore, fast electron diffusion is necessary for superior DSCs. In a traditional nanocrystalline $TiO_2$ mesoporous electrode film, the $TiO_2$ particles are not densely packed, and thus the length of the electron path to the conducting substrate is longer, increasing dissipation at the interfaces. It has now been proven that this issue can be addressed by employing vertically aligned 1D $TiO_2$ NROD and nanotube (NT) array photoanodes.[3] The electrons can easily pass along the NRODs or NTs to the transparent conducting oxide (TCO) electrode. However, the low surface area and inferior dye adsorption of the NRODs have prevented high efficiencies from being achieved. For further improvement of the performance of DSCs, novel aligned 1D $TiO_2$ nanostructures need to be developed, which should combine the merits of both fast electron pathways and high surface area for sufficient dye adsorption. Moreover, though rutile $TiO_2$ is the thermodynamically most stable form, anatase is the preferred structure in DSCs, because it has a larger bandgap and a higher conduction band edge energy. These lead to a higher Fermi level and higher open circuit voltage ($V_{oc}$) in DSCs for the same conduction band electron concentration.[2b] If we would like to utilize the stability of rutile $TiO_2$, a suitable band structure modification is necessary.

Fabrication of 1D nanoscale materials, such as NWs, NTs and NRODs, has gained considerable attention owing to the intrinsic interest in the significance of these structures and the potential for developing nanodevices. These 1D nanostructures provide

[a]*Institute for Superconducting and Electronic Materials, University of Wollongong, Innovation Campus, Squires Way, North Wollongong, NSW 2500, Australia. E-mail: jhk@uow.edu.au*
[b]*Australian Institute for Bioengineering and Nanotechnology, The University of Queensland, St. Lucia, Brisbane, QLD 4072, Australia*
† Electronic supplementary information (ESI) available. See DOI: 10.1039/c2ce00014h

unique electronic properties, such as high electron mobility or quantum confinement effects, high specific surface area, and even high mechanical strength, and have shown fascinating new properties and features.[3] Moreover, the 1D nanostructures show improved reaction/interaction activity because of quantum size effects and the strong contribution of surface reconstruction and surface curvature, which thus make the system more effective and even allow for entirely novel reaction pathways.[3,4] However, the crystal structure and symmetry of both anatase and rutile $TiO_2$ make the growth of oriented anisotropic single-crystalline $TiO_2$ arrays very difficult.[4b] In particular, the synthesis of 1D $TiO_2$ nanostructures with controllable morphology is extremely hard to achieve. To date, only a few studies have reported the heterogeneous growth of oriented single-crystalline $TiO_2$ NRODs or NWs.[4,5]

In this study, therefore, we describe a facile hydrothermal method for controlled growth of oriented 1D single-crystalline $TiO_2$ nanostructure arrays with continually tunable morphologies. By adjusting the hydrolysis rate of the Ti-containing precursor, oriented 1D $TiO_2$ arrays in forms that vary from NRODs to NRIBs, and then NWs have been successfully synthesized. Different morphology could influence the electronic structure and surface chemical activity of the 1D nanostructure arrays, such as band structure, specific surface area, charge transport and recombination, *etc.* The morphology-induced band structure shift would give rutile $TiO_2$ a comparable electronic structure to that of anatase phase, and thus endow it with an enhanced electrochemical performance. *Via* this investigation, it is expected to achieve an insight into nano-architecture design of new morphologies, and to provide a new way to improve the chemical activity of rutile $TiO_2$ by modulating its band structure.

## Results and discussion

Oriented 1D $TiO_2$ nanostructure arrays with controlled morphology were grown on the fluorine-doped tin oxide ($SnO_2$:F, FTO) transparent glass substrates by a hydrothermal approach, as illustrated in Fig. 1. In the synthesis, an aqueous titanium tetraisopropoxide (TTIP) solution ($TTIP_{aq}$) was prepared by mixing TTIP, hydrochloric acid (HCl), and cetyltrimethyl ammonium bromide (CTAB) in de-ionized water in the desired ratio. In some cases, urea was added into the aqueous solution to adjust the pH value. Then, the aqueous TTIP solution was mixed with ethylene glycol (EG) and transferred into autoclaves with cleaned FTO substrates for hydrothermal treatment. When the FTO substrates were immersed in the reaction solutions, titanium hydrates formed by TTIP hydrolysis would condense on the FTO surface, and small $TiO_2$ growth centres or seeds were created during the initial hydrothermal process (Fig. 1(a)). Depending on the growth conditions, three types of 1D $TiO_2$ nanostructures were obtained. When the reaction solution was the aqueous TTIP solution ($TTIP_{aq}$), the orientated 1D $TiO_2$ nanostructures had the typical morphology of rectangular NRODs, as shown in Fig. 1(b). The scanning electron microscope (SEM) image (Fig. 1(c)) reveals that the entire surface of the FTO was covered very uniformly with $TiO_2$ NRODs. With EG added into the aqueous TTIP solution as a non-aqueous co-solvent (Fig. 1(d)), the 1D $TiO_2$ nanostructure grew in the form

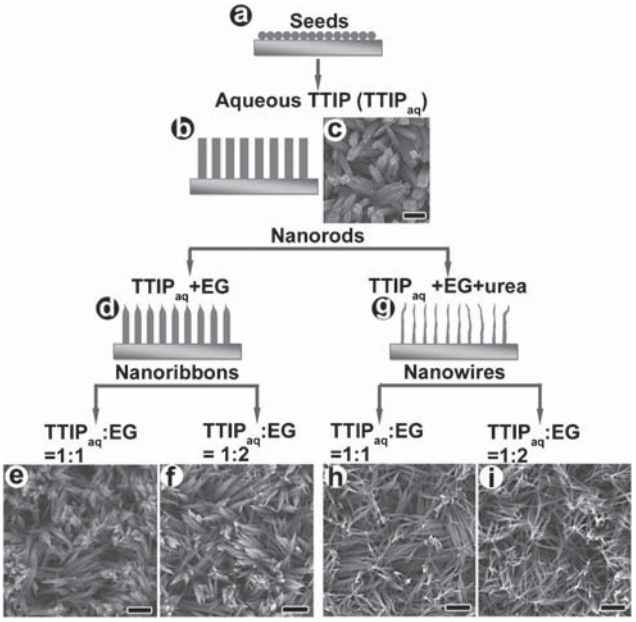


**Fig. 1** Schematic drawing and SEM images of oriented 1D $TiO_2$ nanostructure arrays synthesized under different conditions, where the morphology of 1D $TiO_2$ nanostructures changes from the form of (b–c) NRODs to (d–f) NRIBs, and then to (g–i) NWs. The scale bar in the images is 200 nm.

of NRIBs, as can be seen in Fig. 1(e) and 1(f). When the reaction solution was further modified by the addition of urea (Fig. 1(g)), the morphology of the oriented 1D $TiO_2$ nanostructures was changed to the form of NWs (Fig. 1(h) and (i)). The synthesis details can also be found in the experimental section.

In the present study, the key innovations in morphology control were achieved though the addition of EG and/or urea for tuning the hydrolysis rate of TTIP during the hydrothermal process. Firstly, 1D $TiO_2$ NROD arrays were prepared from the aqueous TTIP solution ($TTIP_{aq}$) as references (Fig. 1(c) and Fig. S1 in the ESI†). The synthesis of rutile $TiO_2$ NROD arrays accounts for the largest portion in all reports on 1D $TiO_2$ nanostructure arrays.[5] The NRODs obtained by wet-chemical approaches are usually in the form of rectangular bars with smooth side walls, but uneven top ends with step edges. This kind of morphology is very typical of rutile $TiO_2$ NRODs obtained from aqueous solution by hydrothermal growth.[4b,5e–f] The tetragonal shape of the rutile NRODs with their step-like square top facet is considered to have resulted from the growth habit of the tetragonal crystal structure. As pointed out by Liu *et al.*, the uneven steps on the top surface indicate that the growth of NRODs proceeds by addition of titanium growth units (*e.g.*, $[Ti(OH)_2Cl_2(OH)_2]$) at the step edges.[4b] Hosono *et al.* reported the growth of rectangular rutile NRODs with similar morphology on a borosilicate glass substrate in solutions containing 10 M NaCl, but they proposed that the addition of NaCl was the key factor for the growth of NROD morphology.[5e] In the present study, the growth of $TiO_2$ NRODs was carried out in aqueous solution with the addition of CTAB surfactant. It is believed that the surfactant is helpful for the aligned growth of $TiO_2$ NRODs. However, according to the previous study carried out by Liu *et al.*, the addition of some common surfactants

including EDA, EDTA, SDS, CTAB and PVP had little effect on the morphology of $TiO_2$ nanorods.[4b] Therefore, the NROD morphology that formed in the aqueous solution is most likely due to the rapid hydrolysis of polymer $TiO_2$ precursor in water, which can provide sufficient titanium hydrate for rapid crystal growth. Therefore, owing to the fast hydrolysis rate of TTIP in aqueous solution during the hydrothermal synthesis, the $TiO_2$ nanocrystals grow rapidly and finally result in the observed shape of rectangular NRODs.

Secondly, the synthesis of 1D $TiO_2$ nanostructure arrays in the form of NRIBs was carried out from a mixed reaction solution of $TTIP_{aq}$ and EG, which is expected to retard the hydrolysis of TTIP during the hydrothermal process. The volume ratios of $TTIP_{aq}$ to EG for the study were 2 : 1, 1 : 1, and 1 : 2, respectively. As shown in Fig. 1(e) and (f), the morphology of the 1D nanostructures that were prepared from the $TTIP_{aq}$ and EG mixed solution were in the shape of NRIBs, which are a much finer structure than NRODs. It is clearly demonstrated that the addition of EG significantly changes the morphology of the 1D $TiO_2$ nanostructures. Compared to the aqueous TTIP solution for NROD preparation, the concentration of TTIP in the mixed solution was only half as great. To exclude the possibility that the change in morphology was promoted by the decreased Ti-precursor concentration, 1D nanostructures prepared from a solution of $TTIP_{aq}$ : $H_2O$ = 1 : 1 was also examined, as is presented in Fig. S2.† The nanostructures obtained from the aqueous solution with half the TTIP concentration still remained in the form of NRODs, except for having a larger size and a shorter length. It is concluded that the changed morphology of the 1D nanostructures is attributable to the addition of EG, not the dilution of the TTIP precursor concentration. The volume ratios of $TTIP_{aq}$ to EG in the reaction solutions show less influence on the morphology of NRIBs. When the nanostructures were synthesized from the solution with $TTIP_{aq}$ : EG = 2 : 1, as shown in the low and high magnification SEM images in Fig. S3,† the nanostructures were mainly in the shape of fine NRIBs 20–40 nm in width, but a few nanostructures having shapes very close to NRODs can be observed. The nanostructure obtained in this solution thus can be treated as a transitional morphology between NRODs and NRIBs, while the 1D nanostructures prepared from the solution with $TTIP_{aq}$ : EG = 1 : 1 were totally in the form of grass-like NRIBs (Fig. S4†). The nanostructures synthesized from the solution with $TTIP_{aq}$ : EG = 1 : 2 were also in the form of grass-like NRIBs, but the NRIBs were bigger than those obtained from $TTIP_{aq}$ : EG = 1 : 1 (Fig. S5†). It has been reported that a biphasic solution with long chain alcohol and acidic CTAB water phase was used for the synthesis of mesostructured $SiO_2$ fibers, since the long chain alcohol can dissolve tetraethyl orthosilicate (TEOS) and separate it from the water phase to reduce the hydrolysis and condensation rates of TEOS.[7] Thus, there is evidence that the 1D $TiO_2$ NRIBs can be synthesized from the water and EG mixed solution, due to its slowing of the hydrolysis rate for TTIP.

Thirdly, oriented 1D $TiO_2$ NW arrays were obtained from the solution with the addition of not only EG, but also 5 mmol urea. Fig. 1(h) and Fig. S6† present the morphology of the nanostructure obtained from the mixed solution with $TTIP_{aq}$ : EG = 1 : 1 combined with 5 mmol urea, wherein the nanostructures had sharp tips like NWs, but were shaped like ribbons at the bottoms, which might be the transitional state between NRIBs and NWs. Fig. 1(i) and Fig. S7† display the morphology of 1D $TiO_2$ arrays hydrothermally synthesized from the solution of $TTIP_{aq}$ : EG = 1 : 2 combined with 5 mmol urea addition. The thin film prepared under these conditions consisted entirely of homogenous NWs with a diameter around 4 nm, by measuring the individual nanowires from the SEM and TEM images. It is well known that the growth of 1D oxide NWs demands a much slower hydrolysis rate of the precursors than that for other 1D nanostructures.[6] Urea is a very weak Brønsted base and highly soluble in water. Its controlled hydrolysis in aqueous solutions can yield ammonium cyanate and gradually, homogenously release $OH^-$ at temperatures higher than 85 °C.[8] As a consequence of the addition of slow-release urea, the pH value of the mixed reaction solution would increase. Although bases have been demonstrated to speed up the condensation reaction, the hydrolysis of TTIP is slowed with increasing basicity, which then results in the growth of $TiO_2$ NWs.[8]

Therefore, during the hydrothermal synthesis, the hydrolysis rate of the TTIP precursor could be adjusted by changing the composition of the reaction solution, and oriented 1D $TiO_2$ nanostructure arrays with a continually adjustable morphology were successfully obtained. The morphology of the 1D $TiO_2$ nanostructures varied from NRODs ($TTIP_{aq}$), to transitional morphology between the NRODs and NRIBs ($TTIP_{aq}$ : EG = 2 : 1), to NRIBs ($TTIP_{aq}$ : EG = 1 : 1 and 1 : 2), and to transitional morphology between the NRIBs and NWs ($TTIP_{aq}$ : EG = 1 : 1 with 5 mmol urea), and then to NWs ($TTIP_{aq}$ : EG = 1 : 2 with 5 mmol urea), with decreasing hydrolysis rate of Ti-containing precursor. This demonstrates the validity of our concept for the morphological control of 1D $TiO_2$ nanostructures by tuning the hydrolysis of precursors.

The X-ray diffraction (XRD) patterns of the obtained 1D $TiO_2$ nanostructure arrays demonstrated that these nanostructures were fully crystallized into rutile phase, and no secondary phase was detectable (Fig. S8†). Moreover, the diffraction peaks revealed the strongly anisotropic growth of the nanostructures, as indicated by the enhanced intensity of the (101) and (002) peaks. Fig. 2 shows cross-sectional SEM views and high resolution transmission electron microscope (HRTEM) observations of the obtained 1D $TiO_2$ nanostructure arrays in the form of NRODs, NRIBs, and NWs. For easy comparison of the performance of these arrays, the length of the $TiO_2$ nanostructures was controlled at around 1 μm. A careful look at the images in Fig. 2(a), (d) and (g) reveals that most of the rutile nanounits are not perpendicular to the substrate surface, but lean toward the azimuthal direction with an angle of around 30°. Because the contact angle between the (101) and the (002) planes is approximately 33°, the side surfaces of the 1D nanostructures should be {110} facets. To further determine the growth direction, individual NRODs, NRIBs and NWs were examined by HRTEM. Fig. 2(b) shows a HRTEM image of an individual NROD crystal. The lattice fringes that are parallel to the side surface can be assigned to rutile (110) planes, because the measured distance between the adjacent fringes coincided well with the crystal spacing $d_{110}$ = 3.247 Å. The NRODs are single crystalline, as evidenced by the sharp selected-area electron diffraction (SAED) pattern (Fig. 2(c)). The labelled SAED

 

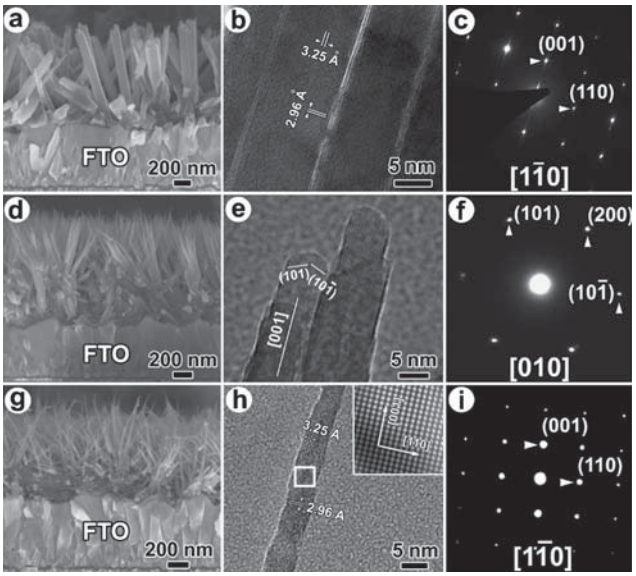


**Fig. 2** Cross-sectional SEM images, TEM images and the corresponding SAED patterns of individual 1D $TiO_2$ nanostructures: (a–c) NROD (aqueous $TTIP_{aq}$), (d–f) NRIB ($TTIP_{aq}$ : EG = 1 : 1), and (g–i) NW ($TTIP_{aq}$ : EG = 1 : 2, 5 mmol urea). The inset in (h) shows an enlargement of the region indicated by the square.

pattern demonstrates that the surface examined is perpendicular to the (110) and (001) plane surfaces ((001) spots can be observed in the SAED patterns because of double reflection). Based on the HRTEM image and the SAED pattern, it is easy to see that the rutile NRODs obtained in this case have grown along the [001] direction. Although no significant difference was found between the XRD patterns for NROD and NRIB thin films, the growth of the NRIBs was changed due to the change in the synthesis environment. As indicated in Fig. 2(e) and (f), the growth of the NRIBs was parallel to the (010) and (100) surface, and the direction was along the [001] crystal orientation. Along the [001] direction, an atomically sharp tip with (101) and (10$\bar{1}$) facets can be observed, which is likely to be the reason why a sharp end tip forms in the NRIBs. The NWs synthesized by the addition of 5 mmol urea have a different microstructure from that of the NRIBs, but it is similar to that of the NRODs. According to the analysis of HRTEM images and SAED patterns (Fig. 2(h) and (i)), the growth of the NWs was along the [001] direction.

It is very clear from the above experiments that the morphology of the aligned rutile $TiO_2$ 1D nanostructures can be tailored by controlling the hydrolysis rate of the polymer precursors. To the best of the authors' knowledge, this is the first systematic work on controlling the morphology of 1D $TiO_2$ nanostructures based on the understanding of the crystal growth mechanism in wet-chemical processing. We therefore argue that our strategic approaches to synthesize 1D $TiO_2$ nanostructure arrays with continuously controllable morphology have numerous benefits in terms of reproducibility, manufacturability, and cost-effectiveness. To explore the possibilities of the oriented 1D $TiO_2$ nanostructure arrays with continuously controllable morphology in photochemical applications, the photovoltaic performance of the oriented 1D $TiO_2$ nanostructure arrays with different morphologies were studied, and the influences of the morphology on the device performance were also investigated.

For comparison of the photovoltaic performance of 1D $TiO_2$ nanostructures with different morphologies, the thickness of the oriented arrays was kept at around 1 μm. We also intended to obtain thin films with appreciable thicknesses by a multilayer assembly process. As shown in Fig. S9,† an oriented NRIB array with a thickness of around 2.5 μm was obtained by repeating the hydrothermal assembly three times. Unfortunately, such long NRIBs were fused at their roots. As a result, a percentage of the surface area gained by increasing the length would be lost. Recently, Xu *et al.* reported a multilayer assembly method to synthesize long ZnO NWs without root fusion.[9] This innovation may also be adopted for the synthesis of long $TiO_2$ 1D nanostructures with high internal surface area.

It is well known that the size and shape of semiconductors have strong influences on their photonic and chemical performances. Fig. 3 presents the effects of the morphology of the 1D $TiO_2$ nanostructure arrays on the band structure, the photoabsorbance in the ultraviolet-visible (UV-Vis) regime, and the kinetic processes in DSCs. Fig. 3(a–c) show the atomic structure of the 1D $TiO_2$ nanostructures, which were built based on the TEM observations in Fig. 2. Interestingly enough, the morphological changes indeed result in shifts in the band structure. Fig. 3(d) displays the UV-Vis spectra of the obtained 1D $TiO_2$ nanostructures. The cut-off edge of the first peak in the NROD array spectrum is around 410 nm, corresponding to the band gap value of 3.0 eV, which is exactly the reported bandgap value of bulk rutile $TiO_2$. Two conspicuous additional absorbance peaks in the range from 400–800 nm were detected in the UV-Vis spectrum of the NRODs. There is a strong scattering effect for visible light, because the size of the NRODs is large enough for light scattering. Compared to the absorption spectrum of NRODs, the cut-off edge of NRIBs shows a slight blue shift to the wavelengths around 405 nm, which is equivalent to a bandgap of 3.07 eV. The light scattering effect also can be found in the spectrum of the oriented NRIB arrays in the visible light regime. This is evidence that a visible light scattering film is helpful to confine the incident light within an electrode.[2b] A photoanode with light scattering will thus enhance the photon-to-current conversion efficiency of solar cells. The UV-Vis spectrum of oriented NW arrays, however, is totally dissimilar to those of the NRODs and NRIBs. A distinct blue shift to 380 nm appeared in the spectrum, demonstrating that the bandgap of the NWs had widened to 3.25 eV. The influence of particle size on the band structure of $TiO_2$ nanoparticles has been studied.[10] The results showed that a particle size on the nanoscale raises the conduction band and lowers the valence band. The widened band-gap shows itself as a blue shift in the absorbance edge in the UV-Vis spectrum. The diameter of the NW synthesized in our study is on the order of 4 nm, which is in the effective size range to produce quantum confinement effects. Therefore, the blue shift observed in the NW UV-Vis spectrum is attributed to the quantum-size effect.

The energy levels of the 1D $TiO_2$ nanostructures, and the kinetic processes in a typical DSC are further explained in Fig. 3(e). In the application of $TiO_2$ semiconductors, rutile is the thermodynamically most stable form. However, anatase is the preferred structure in DSCs, because of its larger band gap (3.2 eV *vs.* 3.0 eV for rutile) and higher conduction band-edge energy. This leads to a higher Fermi level and $V_{oc}$ in DSCs for

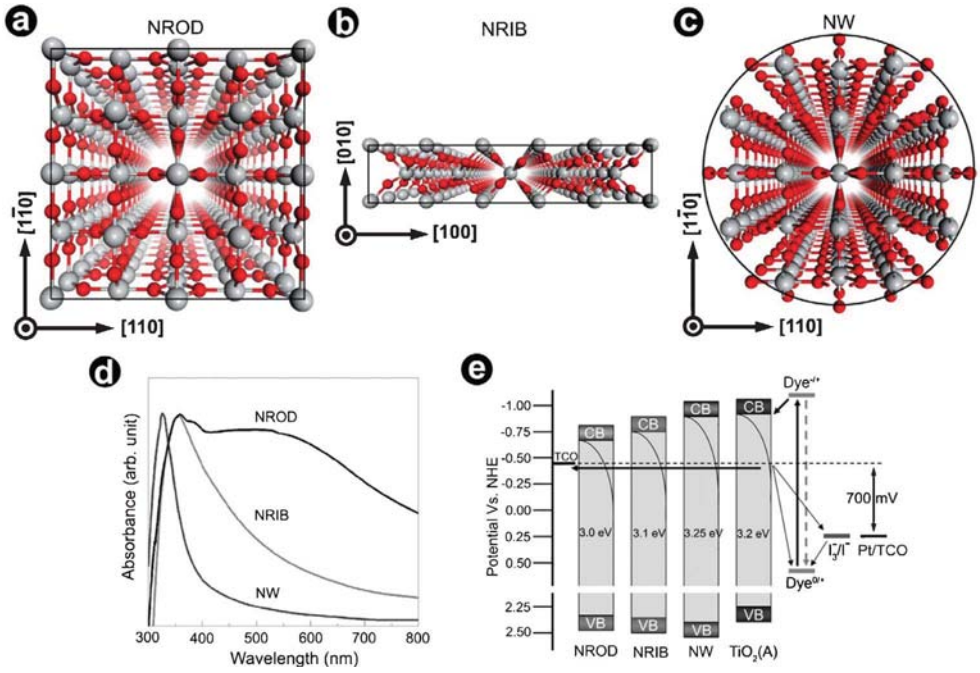


**Fig. 3** Atomic and band structures of 1D $TiO_2$ nanostructures: (a–c) diagram of atomic structure of NROD, NRIB and NW based on the TEM observation. (d) UV-Vis spectra of the NROD, NRIB and NW arrays. (e) Energy band diagrams and kinetic processes in DSCs with NROD, NRIB and NW photoanodes. As a reference, the energy level of anatase $TiO_2$ ($TiO_2$(A)) was also incorporated.

the same conduction band electron concentration. As shown in Fig. 3(e), the band structure of the rutile was widened and shifted by the change of morphology, and was comparable to that of bulk anatase phase. The shift of band structure of the rutile will influence the electron injection, charge transport, and charge recombination, and thus influence the DSC performance.[11] Here, we tested the photovoltaic performance of the oriented 1D $TiO_2$ nanostructure arrays in dye-sensitized solar cells. FTO substrates covered with $\sim$1 μm long oriented 1D $TiO_2$ nanostructure arrays were converted to photoanodes for DSCs by immersion overnight in a 0.5 mM solution of commercially available N719 dye (Sigma-Aldrich). A conductive glass substrate coated with Pt was used as the counter-electrode. The performances of the assembled 1D nanostructure array solar cells were measured under air mass (AM) 1.5 simulated sunlight with a power density of 100 mW cm$^{-2}$.

The measured results on the 1D nanostructure array solar cells, including the short-circuit current density ($J_{sc}$), open-circuit voltage ($V_{oc}$), fill factor ($F$), and energy conversion efficiency ($\eta$), are summarized in Table 1. Fig. 4 shows the typical photocurrent density–photovoltage ($J$–$V$) curves (Fig. 4(a)) and the external quantum efficiencies in the 400–800 nm wavelength range (Fig. 4(b)) of the solar cells made from the oriented 1D $TiO_2$ arrays with different morphologies. It is clear that the shape and size of the nanostructures had significant influences on the photovoltaic performance. Under the illumination of AM 1.5 simulated sunlight, the NROD cell exhibited a short circuit current of 1.63 mA cm$^{-2}$, an open circuit voltage of 0.58 V, and a fill factor of 0.58. The overall conversion efficiency was found to be 0.8%. The external quantum efficiency was $\sim$10% at the peak of dye absorption, around 530 nm for N719 dye. At the same time, not only the $J_{sc}$, $V_{oc}$, and $F$, but also the conversion efficiency $\eta$ of the NRIB and NW solar cells were much higher than those of the NROD solar cells. In particular, the NRIB array cells showed the best performance. The fill factor of the NRIB photoanode was 0.63, and the efficiency was 2.1%, more than two times higher than that of the NROD array cell. The peak external quantum efficiency of the NRIB cell at 530 nm was around 25%.

**Table 1** Photovoltaic performances of the dye-sensitized solar cells with photoanodes made from oriented 1D $TiO_2$ nanostructure arrays having different morphologies

| Morphology | $V_{oc}$ (V) | $J_{sc}$ (mA cm$^{-2}$) | $F$ | $\eta$ (%) |
|---|---|---|---|---|
| Nanorod | 0.57 | 1.63 | 0.58 | 0.8 |
| Nanowire | 0.68 | 4.09 | 0.56 | 1.6 |
| Nanoribbon | 0.63 | 5.35 | 0.63 | 2.1 |

The superior performance of the NRIB solar cells may be the result of the structural features of NRIBs. Firstly, the UV-Vis

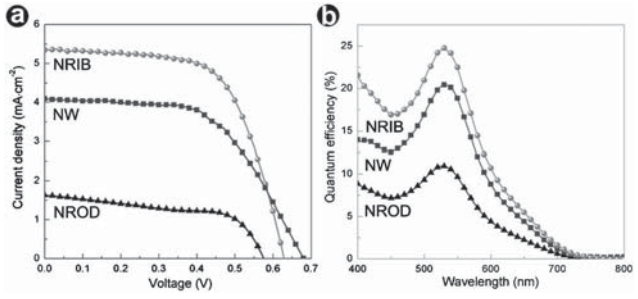


**Fig. 4** (a) Photocurrent–photovoltage characteristics and (b) incident photon to current efficiency (IPCE) of DSCs with photoanodes assembled from oriented 1D $TiO_2$ nanostructure arrays.

spectrum of NRIB arrays demonstrated that they also have as strong a scattering effect in the visible light range as that of NROD arrays, because the width of NRIBs is large enough for light scattering. Secondly, the oriented NRIB arrays possess higher surface area for sufficient dye loading than the NROD arrays, due to the much thinner nanostructure thickness, indicated by the dye-adsorption amount data shown in Fig. S10.† Thirdly, the NRIBs show the presence of abundant sharp edges and tips in their structure, which are the active sites for electrochemical reaction and dye adsorption.[12] Finally and most importantly, the rutile NRIBs have a comparable bandgap and conduction band edge height to those of the chemically active anatase phase. As mentioned above, the band structures of rutile NWs and NRIBs were modified by the change in morphology. According to the heights of conduction band edge, the $V_{oc}$ of the corresponding DSCs should be in the order of $V_{NROD} > V_{NRIB} > V_{NW}$, which coincided well with our measured open voltages. Therefore, the morphology of the oriented 1D NRIB arrays, which possess not only fruitful chemically active sharp edges/tips, but also an improved bandgap and conduction band edge, can give rise to higher electrochemical activity and a higher Fermi level of the semiconductor, and thereby, better performance of devices.

## Conclusions

In conclusion, by rational design, oriented 1D rutile $TiO_2$ nanostructure arrays with continually adjustable morphologies were successfully fabricated by a simple hydrothermal treatment with the assistance of a surfactant. Controlled growth of the well-defined nanostructures on the FTO substrates, namely, NRODs, NRIBs, and NWs, was achieved, based on the concept that the hydrolysis rate of the titanium polymer precursor determines the crystal growth behaviour. The slower the hydrolysis rate, the finer the 1D nanostructure is. This finding has paved the way towards nano-architectures with controlled morphologies based on a good understanding of the crystal growth mechanism. Some other new $TiO_2$ nanostructures are expected to be discovered on the basis of our strategy. The variation of the morphology induced significant change in the band structures of the rutile nanostructures, making them comparable to that of the bulk anatase phase. Under the same test conditions, the NRIB arrays possess fruitful chemically active sharp edges/tips, and good light scattering in the visible light range, but also improved bandgap and conduction band edge height, thus presenting the best photon-to-energy conversion efficiency compared with the other morphologies. This family of well-controlled oriented $TiO_2$ 1D nanostructure arrays is also highly likely to be used in other fields, in superior sensors, field emission devices, photocatalysis, *etc.*

## Experimental

### Synthesis of 1D $TiO_2$ nanostructure arrays on FTO substrates

In a typical synthesis, aqueous TTIP solution was obtained by mixing 0.17 g TTIP, 13.80 g concentrated HCl, 27.3 ml distilled water and 0.15 g CTAB with strong stirring. Then the aqueous TTIP solution mixed with EG in a preset volume ratio of 1 : 0, 2 : 1, 1 : 1, and 1 : 2, respectively, to form the reaction solution for hydrothermal synthesis. For the nanowire arrays preparation, 5 mmol urea was also added. After synthesis, the FTO substrate was taken out and rinsed thoroughly with distilled water.

### Characterization

Phase compositions of the 1D $TiO_2$ nanostructure arrays were measured with a powder X-ray diffractometer (XRD, MMA, GBC Scientific Equipment LLC, Hampshire, IL, USA) with Cu Kα radiation and a LabRam-HR 800 Raman microspectrometer (Horiba Jobin Yvon, Longjumeau Cedex, France). The morphology of the samples was observed with a scanning electron microscope (SEM, JSM-7500FA, JEOL, Tokyo, Japan). The details of the nanostructures were examined with a high resolution transmission electron microscope operated at 200 kV (JEM-2011F, JEOL, Tokyo, Japan). UV-Vis absorption spectra were collected with a UV-Visible light absorption spectroscope in the wavelength range of 200–800 nm (Perkin-Elmer 1600, USA).

### Assembling and testing of dye-sensitized solar cells

Dye absorption was carried out by immersing the FTO substrates loaded with the 1D $TiO_2$ nanostructure arrays into ethanol-based commercial N719 (Sigma-Aldrich) dye solution at 25 °C for 24 h. The dye adsorption amount was determined by measuring the UV-Vis absorption spectrum of the dye-desorbing solution, which obtained by immersing the photoanodes into 5 mL 0.01 M NaOH solution. The solar cells were prepared by assembling a Pt counter-electrode and a dye-adsorbed photoanode made from the 1D $TiO_2$ nanostructure arrays, and then sealing the assembly by using a Surlyn (Dupont) thermoplastic frame (25 μm thick). The assembled cell was filled with a commercial electrolyte purchased from Solaronix (Iodolyte AN-50), and then the cell was sealed again. The active area of the solar cell for testing was 0.0237 $cm^2$. Photocurrent density–voltage ($J$–$V$) characteristics were measured by exposing the cell to AM 1.5 simulated sunlight from a solar simulator (PEL-L12, Peccell Technologies, Japan) combined with a Keithley 2400 source meter. Incident photon-to-current quantum conversion efficiency (IPCE) was measured as an action spectrum, which uses an optical fiber (3 μm diameter) for monochromatic irradiation (PEC-S20DC, Peccell Technologies, Japan). Monochromatic photocurrent was monitored by the continuous irradiation (dc measurement) method.

## Acknowledgements

This work was supported by Australian Research Council Discovery Project DP1096546. ZQS was supported by an Australian Postdoctoral Research (APD) Fellowship.

## References

1 (*a*) X. Chen and S. S. Mao, *Chem. Rev.*, 2007, **107**, 2891–2959; (*b*) G. Liu, L. Z. Wang, H. G. Yang, H. M. Cheng and G. Q. Lu, *J. Mater. Chem.*, 2010, **20**, 831–843; (*c*) A. P. Alivisatos, *Science*, 1996, **271**, 933–937; (*d*) K. Shankar, J. I. Basham, N. K. Allam, O. K. Varghese, G. K. Mor, X. Feng, M. Paulose, J. A. Seabold, K. Choi and C. A. Grimes, *J. Phys. Chem. C*, 2009, **113**, 6327–6359; (*e*) S. Ding, J. S. Chen and X. W. Lou, *Adv. Funct. Mater.*, 2011, **21**, 4120–4125; (*f*) S. Bao, C. Li, J. Zang, X. Cui, Y. Qiao and J. Guo, *Adv. Funct. Mater.*,

2008, **18**, 591–599; (*g*) Z. Sun, J. Kim, Y. Zhao, F. Bijarbooneh, V. Malgras and S. Dou, *J. Am. Chem. Soc.*, 2011, **133**, 19314–19317.
2 (*a*) M. Graetzel, *Inorg. Chem.*, 2005, **44**, 6841–6851; (*b*) A. Hagfeldt, G. Boschloo, L. Sun, L. Kloo and H. Pettersson, *Chem. Rev.*, 2010, **110**, 6595–6663.
3 (*a*) G. Yuan, K. Aruda, S. Zhou, A. Levine, J. Xie and D. Wang, *Angew. Chem., Int. Ed.*, 2011, **50**, 2334–2338; (*b*) X. Feng, K. Shankar, O. K. Varghese, M. T. Paulose, J. Latempa and C. A. Grimes, *Nano Lett.*, 2008, **8**, 3781–3786; (*c*) G. K. Mor, O. K. Varghese, M. Paulose, K. Khankar and C. A. Grimes, *Sol. Energy Mater. Sol. Cells*, 2006, **90**, 2011–2168; (*d*) P. Roy, S. Berger and P. Schmuki, *Angew. Chem., Int. Ed.*, 2011, **50**, 2904–2939; (*e*) Y. Wang, H. Joyce, Q. Gao, X. Liao, H. Tan, J. Zou, S. Ringer, Z. Shan and C. Jagadish, *Nano Lett.*, 2011, **11**, 1546–1549; (*f*) J. Boucle, S. Chyla, M. Shaffer, J. Durrant, D. Bradley and J. Nelson, *Adv. Funct. Mater.*, 2008, **18**, 622–633.
4 (*a*) S. H. Ko, D. Lee, H. W. Kang, K. H. Nam, J. Y. Yeo, S. J. Hong, C. P. Grigoropoulos and H. J. Sung, *Nano Lett.*, 2011, **11**, 666–671; (*b*) B. Liu and E. S. Aydil, *J. Am. Chem. Soc.*, 2009, **131**, 3985–3990; (*c*) M. L. Law, E. Greene, J. C. Johnson, R. Saykally and P. D. Yang, *Nat. Mater.*, 2005, **4**, 455–459.
5 (*a*) J. J. Wu and C. C. Yu, *J. Phys. Chem. B*, 2004, **108**, 3377–3379; (*b*) J. M. Wu, H. C. Shin and W. T. Wu, *Nanotechnology*, 2006, **17**, 105–109; (*c*) C. A. Chen, Y. M. Chen, A. Korotcov, Y. S. Huang, D. S. Tsai and K. K. Tiong, *Nanotechnology*, 2008, **19**, 075611; (*d*) C. C. Weng, K. F. Hsu and K. H. Wei, *Chem. Mater.*, 2004, **16**, 4080–4086; (*e*) E. Hosono, S. Fujihara, K. Kakiuchi and H. Imai, *J. Am. Chem. Soc.*, 2004, **126**, 7790–7791; (*f*) K. Kakiuchi, E. Hosono, H. Imai, T. Kimura and S. Fujihara, *J. Cryst. Growth*, 2006, **293**, 541–545; (*g*) X. J. Feng, J. Zhai and L. Jiang, *Angew. Chem., Int. Ed.*, 2005, **44**, 5115–5118; (*h*) H. Wang, Y. Bai, Q. Wu, W. Zhou, H. Zhang, J. Li and L. Guo, *Phys. Chem. Chem. Phys.*, 2011, **13**, 7008–7013.
6 (*a*) Y. Wan and D. Y. Zhao, *Chem. Rev.*, 2007, **107**, 2821–3361; (*b*) M. Z. C. Hu, M. T. Harris and C. H. Byers, *J. Colloid Interface Sci.*, 1998, **198**, 87–99; (*c*) D. Y. Zhao, J. Y. Sun, Q. Z. Li and G. D. Stucky, *Chem. Mater.*, 2000, **12**, 275–279.
7 (*a*) Q. S. Huo, D. Y. Zhao, J. L. Feng, K. Weston, S. K. Buratto, G. D. Stucky, S. Schacht and F. Schuth, *Adv. Mater.*, 1997, **9**, 974–978; (*b*) Y. Y. Wu, G. S. Cheng, K. Katsov, S. W. Sides, J. F. Wang, J. Tang, G. H. Fredrickson, M. Moskovits and G. D. Stucky, *Nat. Mater.*, 2004, **3**, 816–822.
8 (*a*) M. R. Othman, Z. Helwani, W. Martunus and J. N. Fernando, *Appl. Organomet. Chem.*, 2009, **23**, 335–378; (*b*) B. E. Yoldas, *J. Mater. Sci.*, 1986, **21**, 1087–1092.
9 C. Xu, J. Wu, U. Desai and D. Gao, *J. Am. Chem. Soc.*, 2011, **133**, 8122–8125.
10 N. Satoh, T. Nakashima, K. Kamikura and K. Yamamoto, *Nat. Nanotechnol.*, 2008, **3**, 106–111.
11 (*a*) S. A. Haque, Y. Tachibana, R. Willis, J. E. Moser, M. Graetzel, D. R. Klug and J. R. Durrant, *J. Phys. Chem. B*, 2000, **104**, 538–547.
12 K. Nakada, M. Fujita, G. Dresselhaus and M. S. Dresselhaus, *Phys. Rev. B: Condens. Matter*, 1996, **54**, 17954.



 